Ab Initio Calculations of the Ground Electronic States of Polyiodide Anions

Stephanie B. Sharp and Gregory I. Gellene*

Department of Chemistry and Biochemistry, Texas Tech University, Lubbock, Texas 79409-1061

Received: September 9, 1996; In Final Form: December 20, 1996[⊗]

Equilibrium bond lengths, harmonic frequencies, electron affinities, and dissociation energies (as appropriate) were determined for I, I^-,I_2, I_2^-, and I_3^- by CCSD(T) and four DFT methods (BLYP, BPW91, B3LYP, and B3PW91) using a basis set consisting of a relativistic effective core potential and a triple-zeta plus 2df polarization functions (ECP-TZ(2df)) for the valence electrons. Comparison of the DFT results with the CCSD(T) results and available experimental information indicates that the B3PW91 approach does particularly well describing the bonding in these species. B3PW91/ECP-TZ(2df) calculations of I_5^- in linear ($D_{\infty h}$) and bent (C_{2v}) geometries indicate that the linear structure is a low-energy transition state lying only about 0.1−0.2 eV above the C_{2v} global minimum-energy structure. Harmonic frequencies and infrared and Raman intensities are calculated for both structures and compared to available experimental information.

Introduction

The structure and spectroscopic properties of polyiodide anions have been the subject of numerous experimental investigations motivated in part by the technological utility of various iodine-doped polymers. Examples include optical polarizers formed from iodine-doped poly(vinyl alcohol) films,[1,2] conducting organic polymers formed from iodine-doped polyacetylene films,[3] and modified high-T_c cuprates.[4] A particularly interesting and technologically relevant feature of polyiodide anions is the strong influence environment can have on their structure. For I_3^-, X-ray crystallography[5−8] has shown that the ion is generally within 6° of linear but that the two I−I bond lengths may may differ by more than 6%. For I_5^-, geometries ranging from linear,[9,10] to a highly bent C_{2v} structure,[11] to an $I_3^-\cdot I_2$ complex[12] have been observed. I_7^- and I_9^- seem to be less variable in the crystalline[13,14] state, exhibiting structures that can be described as $I_2\cdot I_3^-\cdot I_2$ and $I_2\cdot I_5^-\cdot I_2$, respectively.

To a large extent the bonding motifs identified for various polyiodide crystals have served as the paradigms for understanding the nature of polyiodides in a noncrystalline environment. A well-known example is the blue-black, "starch−iodine" adduct, the chromophore of which was shown to be linear I_5^- by comparing its Raman and Mössbauer spectra to those of polyiodide crystals.[15] However, in some cases this spectroscopic "fingerprinting" approach can have ambiguities, particularly if more than one polyiodide species is present. Moreover, little or no thermochemical information is available for the polyiodide anions, hampering understanding of polyiodide chain formation. As a first step toward addressing these questions, the equilibrium geometry and harmonic frequencies of I_3^- and I_5^- have been determined by high-level *ab initio* calculations. Previous *ab initio* studies of these species[16] have focused on bonding properties without addressing vibrational frequencies or spectral intensities. Thus, the present work provides the first comparison of theory and experiment for the frequencies and assignments of I_3^- and I_5^- infrared and Raman spectra.

Method

Coupled cluster theory[17,18] at the single and double excitation level with a perturbative treatment of triple excitations (CCSD(T))[19] is one of the most powerful, generally available approaches for building electron correlation onto a single-determinant reference wave function. Unfortunately, CCSD(T) studies of I_5^- and larger polyiodide anions are not currently practical. Alternatively, density functional theory (DFT)[20] can be practically applied to very large systems; however, the range of chemical systems for which the results are accurate[21] is not as established as CCSD(T). Thus, we adopted the following approach. Equilibrium geometries, dissociation energies, and harmonic frequencies for I_2, I_2^-, and I_3^- were calculated using several DFT methods and compared to CCSD(T) results. Taking these molecules as representative of the electronic interactions occurring in polyiodide anions, the comparisons indicate the level of accuracy that can be expected for the DFT calculations of I_5^- and larger polyiodide anions. Four DFT methods, BLYP,[22,23] BPW91,[24] B3LYP,[25] and B3PW91,[26] the later two being so-called hybrid methods, were considered.

Several basis sets were used in this study. The DFT/CCSD(T) comparison calculations and subsequent DFT calculations of I_5^- utilized a high-quality iodine basis[27] set developed to study IHI^-. This set is composed of a relativistic effective core potential[28] and an even tempered (7s7p4d3f) basis set contracted to [3s3p2d1f] for the valence electrons and will be denoted ECP-TZ(2df). All calculations were performed using the Gaussian 94 suite of programs[29] in which analytical energy derivatives are unavailable for DFT calculations using basis sets containing f functions in combination with an effective core potential and for all CCSD(T) calculations. Thus, all geometry optimizations and harmonic frequencies determined with the ECP-TZ(2df) basis set were obtained using numerical derivatives.

It also of interest to calculate infrared absorption and Raman scattering intensities which are best accomplished using analytical energy derivatives. Thus, these properties were calculated using DFT methods with an all-electron split-valence basis set[30] denoted SV4. This set is composed of (16s15p7d) basis functions contracted to [6s5p2d] and augmented with either 2d (denoted SV4(2d))[30] or a 3s2p3d2f (denoted SV4(3s2p3d2f)) diffuse set of functions. Because SV4(3s2p3d2f) was developed specifically for *ab initio* studies of I_2 polarizability,[31] it should be well-suited for use in determining Raman scattering intensities and provides a check of the results obtained with the smaller SV4(2d) basis set. In all calculations, only pure spherical harmonic basis sets were employed.

[⊗] Abstract published in *Advance ACS Abstracts,* February 15, 1997.

S1089-5639(96)02755-7 CCC: $14.00

TABLE 1: Calculated Energy (*E*) and Electron Affinity (EA) for I and I^-

				EA(I) (eV)	
method	basis set	$E(I^-)$ (au)	E(I) (au)	without SO	with SO[a]
CCSD(T)	ECP-TZ(2df)	−11.431 971 7	−11.317 487 3	3.12	2.81
BLYP	ECP-TZ(2df)	−11.443 394 2	−11.329 817 8	3.09	2.75
BPW91	ECP-TZ(2df)	−11.505 519 3	−11.387 712 7	3.21	2.90
B3LYP	ECP-TZ(2df)	−11.486 788 4	−11.366 882 9	3.26	2.95
B3PW91	ECP-TZ(2df)	−11.510 549 5	−11.390 347 5	3.27	2.96
B3PW91	SV4(2d)	−6915.778 199 7	−6915.655 634 2	3.33	3.02
CCSD(T)	SV4(2d)	−6913.121 064 0	−6913.007 599 2	3.09	2.78
B3PW91	SV4(3s2p3d2f)	−6915.781 281 4	−6915.657 472 7	3.37	3.06
expt[b]					3.06

[a] The effect of spin−orbit (SO) interaction is included as described in the text. [b] Reference 32.

TABLE 2: Calculated Spectroscopic Properties and Total Energy for I_2^-

					D_e (eV)	
method	basis set	E (au)	r_e (Å)	ω_e (cm^{-1})	without SO	with SO[a]
CCSD(T)	ECP-TZ(2df)	−22.788 036 3	3.2995	105.5	1.050	0.800
BLYP	ECP-TZ(2df)	−22.822 073 7	3.4892	73.0	1.330	1.080
BPW91	ECP-TZ(2df)	−22.943 961 8	3.3714	84.4	1.380	1.133
B3LYP	ECP-TZ(2df)	−22.899 436 3	3.4012	85.3	1.245	0.995
B3PW91	ECP-TZ(2df)	−22.948 289 0	3.3226	93.7	1.290	1.040
B3PW91	SV4(2d)	−13831.487 170 6	3.3104	92.6	1.317	1.067
CCSD(T)	SV4(2d)	−13826.171 567 2	3.3104[b]		1.167	0.917
B3PW91	SV4(3s2p3d2f)	−13831.492 380 4	3.2624	100.7	1.459	1.209
expt[c]			3.23[c]	115[c,d]		1.06,[c] 1.18[e]

[a] The effect of spin−orbit (SO) interaction is included as described in the text. [b] Geometry not reoptimized. [c] Reference 38. [d] Reference 37. [e] Reference 39.

TABLE 3: Calculated Spectroscopic Properties and Total Energy for I_2

					D_e (eV)		EA (eV)	
method	basis set	E (au)	r_e (Å)	ω_e (cm^{-1})	without SO	with SO[a]	without SO	with SO[a]
CCSD(T)	ECP-TZ(2df)	−22.698 508 1	2.7090	210.2	1.73	1.12	2.44	2.49
BLYP	ECP-TZ(2df)	−22.726 083 8	2.7358	198.8	1.81	1.20	2.61	2.66
BPW91	ECP-TZ(2df)	−22.848 705 5	2.7033	212.2	1.99	1.68	2.59	2.65
B3LYP	ECP-TZ(2df)	−22.798 143 9	2.7064	211.8	1.75	1.14	2.76	2.81
B3PW91	ECP-TZ(2df)	−22.850 272 7	2.6845	221.6	1.89	1.28	2.67	2.72
B3PW91	SV4(2d)	−13831.384 513	2.7021	216.6	1.99	1.38	2.79	2.84
CCSD(T)	SV4(2d)	−13826.075 593			1.64	1.03	2.61	2.66
B3PW91	SV4(3s2p3d2f)	−13831.395 825 6	2.6651	227.1	2.20	1.59	2.63	2.65
expt[b]			2.6663	214.5		1.56		2.55

[a] The effect of spin−orbit (SO) interaction is included as described in the text. [b] Reference 41.

Results and Discussion

Computational results for I and I^- are listed in Table 1. When spin−orbit (SO) effects are not included, all of the methods investigated give an iodine electron affinity that is larger than the experimental value[32] with CCSD(T) results appearing to be generally more accurate than DFT results. However, in the case of iodine, spin−orbit effects on the electron affinity are substantial, being given by $^1/_3[E(^2P_{3/2}) - E(^2P_{1/2})] = 0.31$ eV.[33] With this correction, the DFT electron affinity results are generally superior to CCSD(T) with the B3PW91/SV4-(3s2p3d2f) result being in exact agreement with experiment. Also, basis set effects on the EA of iodine are small with the calculated value varying by only 1−3% in CCSD(T) and B3PW91 calculations with different basis sets.

Computational results for I_2^- (Table 2) are comparable to those obtained in previous *ab initio* studies.[34−36] Comparing the results in Table 2 for r_e and ω_e obtained with the ECP-TZ-(2df) basis set to experiment,[37−39] the performance of CCSD(T) is found to be superior to the DFT methods investigated. Also, the hybrid DFT methods (B3LYP and B3PW91) are found to be superior to their nonhybrid counterparts (BLYP and BPW91) with the ECP-TZ(2df) basis set. Before the calculated results for D_e can be compared properly to the experimental value, a correction for SO interaction is again required. A semiempirical treatment[40] indicates that SO effects will decrease the calculated D_e by about 0.25 eV. When this correction is applied, all D_e values calculated with the DFT methods investigated are closer to the experimental value than are the CCSD(T) results. The D_e results obtained in the B3PW91/SV4(3s2p3d2f) calculations appear particularly close to the most recent experimental value.[39] However, this agreement may be fortuitous because D_e obtained with the ECP-TZ(2df) and SV4(2d)basis sets are about 0.15 eV smaller. In other more extensive multireference configuration interaction calculations[40] which will be reported elsewhere, a D_e of 1.17 eV is obtained.

Computational results for I_2 are summarized in Table 3. Comparing the calculated results for r_e and ω_e to the experimental values,[41] CCSD(T) and the DFT methods are seen to be comparably accurate. The calculated values for D_e and EA again require a correction for spin−orbit interaction before they can be properly compared to experiment. Recent relativistic calculations of Teichteil and Pelissier[42] indicate that the lowering of the ground state potential curve due to spin−orbit effects does not exceed 0.01 eV in the vicinity of r_e. Thus, correcting for spin−orbit effects lowers the calculated D_e by 0.61 eV and raises the calculated EA by about 0.05 eV. When these corrections are applied, the CCSD(T) calculations are found to significantly underestimate D_e. Similiar results have been

TABLE 4: Calculated Spectroscopic Properties and Total Energy for I_3^-

method	basis set	E (au)	r_e (Å)	$D_e(I_2 + I^-)$ (eV)	$\omega_1(\sigma_g)$ (cm^{-1})	$\omega_2(\pi_u)$ (cm^{-1})	$\omega_3(\sigma_u)$ (cm^{-1})
CCSD(T)	ECP-TZ(2df)	−34.173 933 3	2.9822	1.18	107.8	58.2	129.3
BLYP	ECP-TZ(2df)	−34.222 091 0	3.0530	1.43	93.3	51.8	121.2
BPW91	ECP-TZ(2df)	−34.409 756 4	2.9926	1.51	102.9	55.6	134.7
B3LYP	ECP-TZ(2df)	−34.333 817 4	3.0051	1.33	102.7	56.1	125.1
B3PW91	ECP-TZ(2df)	−34.412 302 1	2.9644	1.40	109.7	58.8	135.8
B3PW91	SV4(2d)	−20747.220 169 1	2.9875	1.56	107.4	62.2	134.1
CCSD(T)	SV4(2d)	−20739.246 490 2		1.36			
B3PW91	SV4(3s2p3d2f)	−20747.232 354 6	2.9513	1.50	111.7	66.2	133.8
				1.02[a]			
expt				1.31[b]	107[c]	74[c]	138[c]

[a] ΔE^{298} determined from the ΔH^{298} value of ref 43. [b] Reference 44. [c] Reference 45.

TABLE 5: Comparison[a] of DFT and CCSD(T) Results with the ECP-TZ(2df) Basis Set

	rms			
DFT method	Δr_e (Å)	$\Delta\omega_e$ (cm^{-1})	ΔD_e (eV)	ΔEA (eV)
BLYP	0.118	17.3	0.18	0.12
BPW91	0.042	10.1	0.31	0.12
B3LYP	0.060	9.6	0.14	0.25
B3PW91	0.022	8.0	0.21	0.19

[a] Root-mean-squared deviation (rms Δ) between the CCSD(T) and the DFT result.

observed for calculations employing multiconfigurational techniques and comparable basis sets.[42] In general, the DFT results agree better with the experimental D_e, but the value may be high or low depending on the particular DFT method and basis set. Again, agreement with experiment may be fortuitous because augmenting the SV4 basis set increases D_e by about 15% in B3PW91 calculations. Comparing the calculated EA values to experiment, the CCSD(T) are generally superior to the DFT methods with the same basis set.

Computational results for I_3^- are summarized in Table 4. With the exception of D_e, comparable values of the spectroscopic constants are determined by the CCSD(T) and DFT methods. For D_e, the CCSD(T)/ECP-TZ(2df) result is comparable to an experimental value[43] which was derived from solution thermochemical measurements whereas the generally larger DFT results are comparable to a recent mass spectrometric determination.[44] Because no high-resolution gas phase spectroscopy has been reported for this ion, the accuracy of the calculated values for r_e and the vibrational frequencies cannot be assessed in detail. However, the calculated frequencies are near those reported[45] for $(CH_3)_4NI_3$, a crystal in which the I_3^- moiety adopts a linear symmetric geometry.

As mentioned in the methods section, the calculations on I, I^-, I_2, I_2^-, and I_3^- were performed principally to established the accuracy of DFT methods on these system. This point is addressed by Table 5, which reports the root-mean-square Δr_e, $\Delta\omega_e$, ΔD_e, and ΔEA calculated with the ECP-TZ(2df) basis set for these molecules where "Δ" is the difference between the CCSD(T) and the DFT result for a particular spectroscopic parameter. Inspection of Table 5 indicates that, of the DFT methods considered, the B3PW91 method best reproduces the CCSD(T) values for r_e and ω_e with a relative deviation of only 0.75% and 6.1%, respectively. Although B3PW91 less successfully reproduces the CCSD(T) values for D_e and EA, these parameters are less accurately determined by the CCSD(T) calculations and are less relevant to the many current condensed phase spectroscopic investigations of polyiodide anions. Thus, because the CCSD(T)/ECP-TZ(2df) results are in good agreement with the available experimental r_e and ω_e values, and because the B3PW91/ECP-TZ(2df) results are in good agreement with the CCSD(T)/ECP-TZ(2df) results, the B3PW91/ECP-TZ(2df) level of theory was selected to study I_5^-.

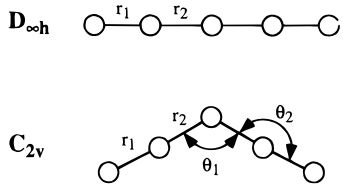

Figure 1. Internal coordinate system used to optimize the structure of the linear ($D_{\infty h}$) and bent (C_{2v}) forms of I_5^-.

The coordinates used to define the geometry of linear and bent I_5^- are shown in Figure 1. Table 6 lists the minimum-energy configuration of linear and bent I_5^- obtained using the ECP-TZ(2df) and SV4(2d) basis sets. Both structures are characterized by inner I−I bonds which are substantially longer than the outer I−I bonds. Similiar results[16] were obtained by a previous study of the C_{2v} structure. However, the central bond angle (θ_1) is found in the present work to be 11−15° larger than the previous computational results[16] and about 26° larger than the experimental value.[46] Because the present result for θ_1 is nearly independent of basis set, the discrepancy between the present and previously calculated[16] value of θ_1 is probably best attributed to the the higher level of electron correlation used in the present study. The difference between the present and crystallographic value for θ_1 may be due to crystal packing forces which could distort I_5^- from its gas phase equilibrium value. This explanation is supported by the small energy difference of 0.08−0.16 eV, depending on the computational method, between the C_{2v} and $D_{\infty h}$ structures, suggesting that very little energy is required to bend the central bond of I_5^-. This small energy difference is also in agreement with the experimental observation of either linear or bent structures of I_5^- depending on the environment.

At each level of theory investigated, the C_{2v} structure was found to have a lower energy than the $D_{\infty h}$ structure. To characterize the nature of these stationary points, harmonic frequencies were calculated. The results for the B3PW91/ECP-TZ(2df) level of theory are listed in Tables 7 and 8 for the $D_{\infty h}$ and C_{2v} structures, respectively, and the form of the normal coordinates is shown in Figure 2. The imaginary frequency of 32.9i cm^{-1} calculated for one of the π_u bending modes of linear I_5^- identifies this structure as a transition state between two equivalent C_{2v} minima which represent the equilibrium structure. However, the ease with which the central angle can be deformed is clearly demonstrated by the very low frequency (11.7 cm^{-1}) and the form of the corresponding normal mode for ω_1 of the C_{2v} structure. Comparing the other modes for the two structures shows that for only one pair of corresponding modes, ω_6 in C_{2v} and ω_4 in $D_{\infty h}$, are the calculated frequencies significantly different. Thus, the two structures would not be readily distinguished on the basis of vibrational frequencies alone.

Of course, a potentially much more powerful method of distinguishing the two structures is provided by the type and

TABLE 6: Minimum-Energy Geometry for I_5^-

geometry	method	basis set	r_1 (Å)	r_2 (Å)	θ_1 (deg)	θ_2 (deg)	D_e (eV)[a]
$D_{\infty h}$	B3PW91	ECP-TZ(2df)	2.833	3.078	180.0	180.0	0.593
$D_{\infty h}$	CCSD(T)	ECP-TZ(2df)	2.833[b]	3.078[b]	180.0	180.0	0.490
$D_{\infty h}$	B3PW91	SV4(2d)	2.852	3.121	180.0	180.0	0.635
C_{2v}	B3PW91	ECP-TZ(2df)	2.857	3.065	120.8	176.7	0.718
C_{2v}	CCSD(T)	ECP-TZ(2df)	2.857[b]	3.065[b]	120.8[b]	176.7[a]	0.571
C_{2v}	B3PW91	SV4(2d)	2.875	3.095	119.7	176.4	0.796
C_{2v}	SCF	3-21G(d)[c]	2.807	3.246	106.5	178.9	
C_{2v}	SCF	ECP-DZ(d)[c]	2.796	3.274	109.2	178.7	
C_{2v}	MP2	ECP-DZ(d)[c]	2.866	3.114	106.0	178.2	
C_{2v}	expt		2.81[d]	3.17[d]	95.0[d]	185.5[d]	0.51[e]

[a] With respect to $I_2 + I_3^-$. [b] Geometry was not reoptimized. [c] Reference 16. [d] Reference 46. [e] Reference 44.

TABLE 7: Calculated[a] Harmonic Frequencies and Infrared and Raman Intensity for Linear I_5^-

		SV4(2d)			
basis set	ECP-TZ(2df) freq (cm^{-1})	freq (cm^{-1})	IR int (km/mol)	Raman int (Å^4/amu)	Raman depolar
$\omega_{1a,b}(\pi_u)$	39.2i	33.6i	(0.09)		
$\omega_{2a,b}(\pi_u)$	26.3	26.7	0.04	0.00	
$\omega_{3a,b}(\pi_g)$	47.4	47.5	0.00	1.77	0.75
$\omega_4(\sigma_g)$	55.5	55.8	0.00	10.86	0.28
$\omega_5(\sigma_u)$	113.9	113.1	144.36	0.00	
$\omega_6(\sigma_u)$	145.7	147.6	239.90	0.00	
$\omega_7(\sigma_g)$	165.0	167.3	0.00	727.22	0.32

[a] At the B3PW91 level of theory.

TABLE 8: Calculated[a] Harmonic Frequencies and Infrared and Raman Intensity for Bent I_5^-

		SV4(2d)			
basis set	ECP-TZ(2df) freq (cm^{-1})	freq (cm^{-1})	IR int (km/mol)	Raman int (Å^4/amu)	Raman depolar
$\omega_1(A_1)$	11.7	13.9	0.04	21.3	0.57
$\omega_2(B_2)$	51.2	53.0	2.82	0.5	0.75
$\omega_3(A_2)$	53.4	55.9	0.00	1.21	0.75
$\omega_4(B_1)$	56.6	57.2	0.03	0.001	0.75
$\omega_5(A_1)$	57.5	60.0	0.62	4.73	0.11
$\omega_6(A_1)$	90.0	89.1	1.62	4.74	0.14
$\omega_7(B_2)$	109.9	112.6	47.68	2.20	0.75
$\omega_8(B_2)$	143.5	144.0	196.01	34.08	0.75
$\omega_9(A_1)$	157.4	158.3	18.8	223.95	0.29

[a] At the B3PW91 level of theory.

number of infrared- and Raman-active modes in each case. To address this point quantitatively, infrared and Raman intensities were calculated at the B3PW91/SV4(2d) level of theory, and the results are listed in Tables 7 and 8 for the $D_{\infty h}$ and C_{2v} structures, respectively. Although recent calculations have demonstrated the accuracy of DFT methods in predicting Raman intensities,[47] there was some concern about the adequacy of the SV4(2d) basis set, particularly regarding Raman intensity calculations which depend on changes in polarizability along the normal coordinates. As a check, infrared and Raman intensities were calculated for I_2^-, I_2, and I_3^- at the B3PW91/SV4(2d) and the B3PW91/SV4(3s2p3d2f) levels of theory. Inspection of Table 9 shows that, with the exception of the open-shell I_2^- ion, the infrared and Raman intensities calculated with the two basis sets agree within about 10%. This agreement suggests that the B3PW91/SV4(2d) calculations should be adequate to predict relative infrared and Raman intensities for the closed-shell I_5^- ion. Comparison of Tables 7 and 8 indicates that the two I_5^- structures can be distinguished in the far-infrared by the intensity ratio of the two strongest absorptions; $I(\omega_6)/I(\omega_5) = 1.7$ for the linear structure and $I(\omega_8)/I(\omega_7) = 4.1$ for the bent structure. The structures could also be distinguished by their Raman spectra, which would be strongly dominated by ω_7 for the linear structure but could contain scattering due to ω_1 and ω_8 at 10−15% of the major ω_9 transition for the bent structure. It should be noted, however, that the Raman spectra of I_5^- shows strong resonance enhancements that are not include in the present calculations.

Comparison to Experiment

Because frequencies and infrared and Raman intensities have been calculated with a harmonic approximation, they are most properly compared to experimentally derived harmonic frequencies. Unfortunately, the available experimental information is not sufficient to determine harmonic frequencies, and comparison must be made to the actual transition frequencies which, of course, are anharmonic. However, considering the relatively small anharmonicity[37,41] exhibited by I_2^- and I_2, a harmonic approximation is expected to be adequate for the high-frequency stretching modes. Alternatively, anharmonic considerations are expected to be more important for bending modes, particularly those having a large projection on the minimum-energy path connecting the C_{2v} and $D_{\infty h}$ structures. Nevertheless, some instructive comparisons to experiment can be made.

Although vibrational transitions have been reported for I_5^- in a variety of environments, the following comparisons to experiment will be limited to cases where the carrier of the spectrum is known to be I_5^-. In particular, we consider the infrared and Raman measurements of crystalline $(CH_3)_4NI_5^-$ (bent I_5^-)[45,48] and $(TMA{\cdot}H_2O)_{10}H^+I_5^-$ (linear I_5^-; TMA = trimesic acid)[48] and the Raman studies[15,48] of $(TMA{\cdot}H_2O)_{10}H^+I_5^-$ and starch−iodine.[15] For bent I_5^-, far-infrared transitions observed[45,48] at 155−160 and 142−145 cm^{-1} were assigned to the modes labeled ω_9 and ω_8, respectively, in Table 8 and Figure 2. These assignments are in excellent agreement with the calculated values of 157.4 and 143.5 cm^{-1}, respectively. Additional far-infrared bands were reported[45,48] for bent I_5^- at 40−50 cm^{-1} attributed to an unassigned bending mode and at 74−76 cm^{-1} which was assigned to ω_7. Of the four bending modes calculated to occur near 50 cm^{-1}, the infrared intensity calculations suggest that the observed bending mode is best assigned to ω_2. In the Raman spectra a transition was observed[45] at 153 cm^{-1} and assigned to ω_9. Additionally, a transition at 112 cm^{-1} was observed[48] and assigned to a symmetric stretch of the inner I−I bonds. Figure 2 shows that this description does not well fit any of the normal modes of bent I_5^-. If ω_7 is taken as assigned to the 76 cm^{-1} mode,[45,48] then ω_6 is the best assignment of the 112 cm^{-1} mode. It is possible that the discrepancies between the observed and calculated frequencies for ω_6 and ω_7 may be due to the much smaller θ_1 and longer r_2 in the crystal structure.

For linear I_5^-, far-infrared transitions have been reported[48] at 90 and 45 cm^{-1} and assigned to the asymmetric stretch of the inner I−I bonds and a bending mode, respectively. Figure 2 indicates that ω_5 corresponds to the asymmetric stretch of the inner I−I bonds. Although ω_6 is calculated to occur about

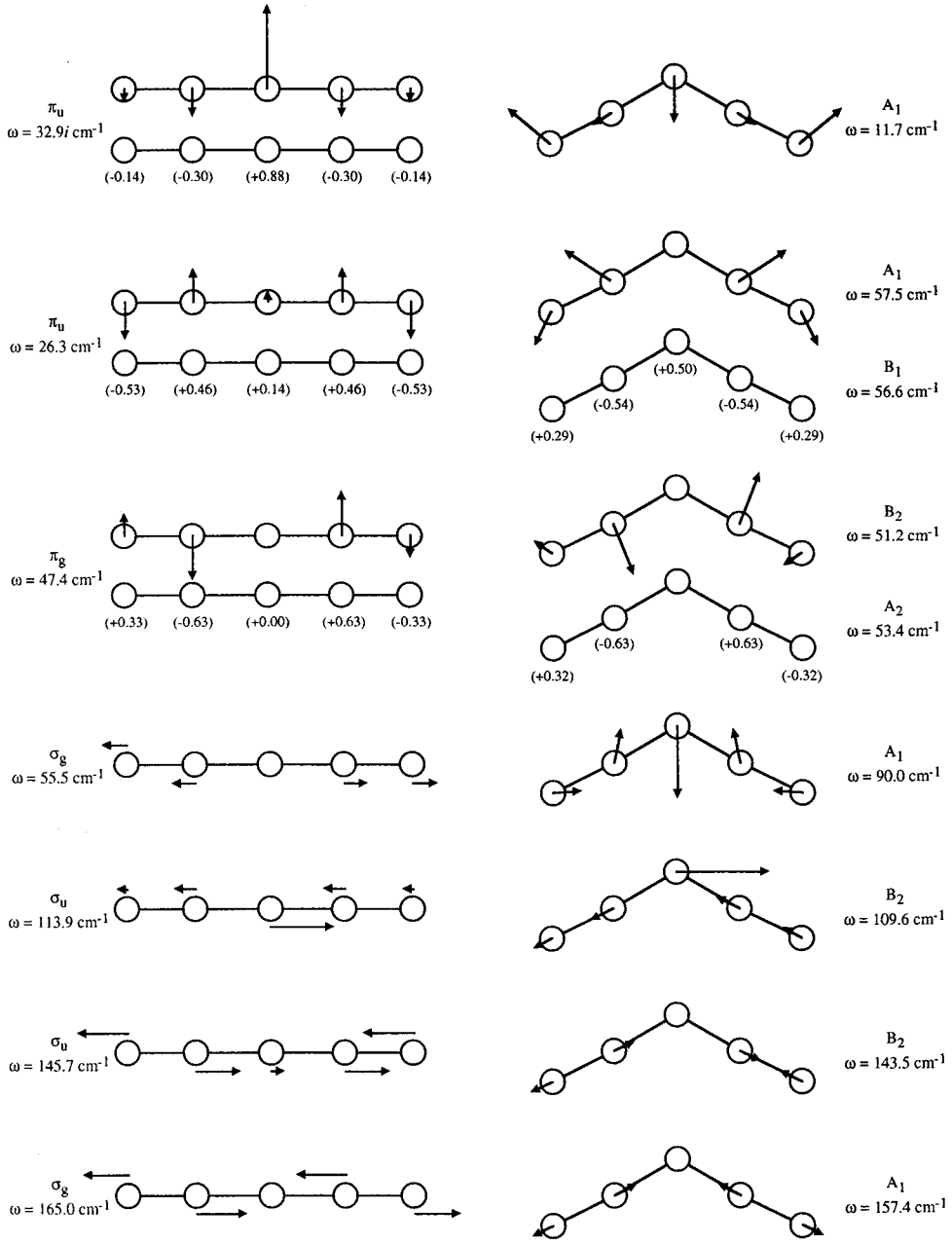

Figure 2. Form of normal mode coordinates for linear and bent I_5^-. Corresponding modes are aligned horizontally.

TABLE 9: Comparison of Calculated[a] I_2, I_2^-, and I_3^- Infrared and Raman Intensity with the SV4(2d) and SV4(3s2p3d2f) Basis Sets

		SV4(2d)			SV4(3s2p3d2f)		
species	mode	IR int (km/mol)	Raman int (Å^4/amu)	Raman depolar	IR int (km/mol)	Raman int (Å^4/amu)	Raman depolar
I_2	ω_1		12.18	0.21		11.40	0.17
I_2^-	ω_1		52.08	0.31		37.13	0.28
I_3^-	ω_1		48.31	0.29		44.19	0.27
I_3^-	ω_2	0.13			0.13		
I_3^-	ω_3	110.5			123.2		

[a] At the B3PW91 level of theory.

24 cm^{-1} above the observed absorption, it is predicted to be a strong transition and remains the best assignment for the 90 cm^{-1} mode. With regard to the 45 cm^{-1} absorption, symmetry considerations indicate that ω_1 and ω_2 are the only two infrared-active bending modes. Because the TMA crystalline environment interacts with the I_5^- bending potential to the point of stabilizing the linear geometry and thus completely altering the gas phase character of ω_1, the calculated frequencies of the bending modes are not very predictive. However, ω_1 and ω_2 span the π_u vibrational space for which the calculated infrared intensities predict very little absorption probability. Thus, the assignment of the 45 cm^{-1} mode to linear I_5^- can be questioned. Raman studies[48] of I_5^- have identified transitions at 165, 104, and 75 cm^{-1} for $(TMA{\cdot}H_2O)_{10}H^+I_5^-$ and transitions[15] of 163, 109, and 56 cm^{-1} for starch−iodine complexes. The transition near 164 cm^{-1} has been assigned[15,48] to the symmetric stretch of the outer I−I bonds, in excellent agreement with the frequency and the form of the normal mode calculated for ω_7.

The transition near 107 cm^{-1} has been assigned alternately to ω_1 of I_3^- (in excellent agreement with the present calculations), occurring as either an impurity or an I_5^- photolysis product,[48] or to the symmetric stretch[15] of the inner I−I bonds of I_5^-. Additionally, the transition at 75 cm^{-1} has also been assigned to the symmetric stretch of the inner I−I bonds of I_5^-. However, the calculations identify this mode as ω_4 with a frequency of 55.5 cm^{-1}. It would seem that the observed transitions are too high to be associated with the fundamental of this mode. Alternatively, the calculations indicate that the previously unassigned transition at 56 cm^{-1} for the starch−iodine complex[15] can be assigned to ω_4, suggesting that the transitions near 107 cm^{-1} may be the first overtone of ω_4 (although the assignment to I_3^- cannot be ruled out). In a similar vein, combination bands observed[15] at 215 and 272 cm^{-1} can be assigned to $\omega_7 + \omega_4$ and $\omega_7 + 2\omega_4$. Noting that long overtone progressions of ω_3 for I_3^- have been observed,[49] the transition at 165 and 272 cm^{-1} may also contain a contribution form $3\omega_4$ and $4\omega_4$, respectively.

Acknowledgment. We thank Dr. C. W. Bauschlicher, Jr., for providing the details of the ECP-TZ(2df) basis set and Professor L. Sutherland for communicating his thermochemical measurements prior to publication. We are also grateful to the National Science Foundation (Grant CHE-9551008) and the Robert A. Welch Foundation for partial support of this research.

References and Notes

(1) Land, E. H. *J. Opt. Soc. Am.* **1951**, *41*, 957.
(2) West, C. D.; Jones, R. C. *J. Opt. Soc. Am.* **1951**, *41* 982.
(3) Salaneck, W. R.; Thomas, H. R.; Bigelow, R. W.; Duke, C. B.; Plummer, E. W.; Heeger, A. J.; MacDiarmid, A. G. *J. Chem. Phys.* **1980**, *73*, 4746.
(4) Faulques, E.; Molinré, P.; Berdahl, P.; Nguyen, T. P.; Mansot, J. *Physica C* **1994**, *219*, 297.
(5) Mooney, R. C. L. *Z. Kristallogr.* **1935**, *90*, 143.
(6) Tasman, H. A.; Boswijk, K. H. *Acta Crystallogr.* **1955**, *8*, 59, 857.
(7) Mooney, R. C. L.; Slater, J. C. *Acta Crystallogr.* **1959**, *12*, 187.
(8) Reddy, J. M., Knox, K.; Robin, M. B. *J. Chem. Phys.* **1964**, *40*, 1082.
(9) Herbstein, F. H.; Kapon, M. *Acta Crystallogr., Sect. A* **1972**, *A28*, 574.
(10) Herbstein, F. H.; Kapon, M.; Reisner, G. M. *Proc. R. Soc. London, A* **1981**, *376*, 301.
(11) Hach, R. J.; Rundle, R. E. *J. Am. Chem. Soc.* **1951**, *73*, 4321.
(12) Herbstein, F. H.; Kapon, M. *Nature (London)* **1972**, *239*, 153.
(13) Havinga, E. E.; Wiebega, E. H. *Acta Crystallogr.* **1958**, *11*, 733.
(14) James, W. J.; Hach, R. J.; French, D.; Rundle, R. E. *Acta Crystallogr.* **1955**, *8*, 814.
(15) Teitelbaum, R. C.; Ruby, S. L.; Marks, T. J. *J. Am. Chem. Soc.* **1980**, *102*, 3322.
(16) Lin, Z.; Hall, M. B. *Polyhedron* **1993**, *12*, 1499.
(17) Čížek, J. *J. Chem. Phys.* **1966**, *45*, 4256.
(18) Bartlett, R. J. *J. Phys. Chem.* **1989**, *45*, 1697.
(19) Raghavachari, K.; Trucks, G. W.; Pople, J. A.; Head-Gordon, M. *Chem. Phys. Lett.* **1989**, *157*, 479.
(20) Parr, R. G.; Yang, W. *Density-Functional Theory of Atoms and Molecules*; Oxford: New York, 1989.
(21) Seminario, J. J., Politzer, P., Eds. *Modern Density Functional Theory: A Tool for Chemistry*; Elsevier: Amsterdam, 1995.
(22) Becke, A. D. *Phys. Rev. A* **1988**, *38*, 3098.
(23) Lee, C.; Yang, W.; Parr, B. G. *Phys. Rev. B* **1988**, *37*, 785.
(24) Perdew, J. P.; Wang, Y. *Phys. Rev. B* **1992**, *45*, 13244.
(25) Stephens, P. J.; Devlin, F. J.; Chabalowski, C. F.; Frisch, M. J. *J. Phys. Chem.* **1994**, *98*, 11623.
(26) Becke, A. D. *J. Chem. Phys.* **1993**, *98*, 5648.
(27) Florance, S.; Schatz, G. C.; Lee, T. J.; Bauschlicher, Jr., C. W. *Chem. Phys. Lett.* **1993**, *202*, 495.
(28) Hay, P. J.; Wadt, W. R. *J. Chem. Phys.* **1985**, *82*, 284.
(29) Gaussian 94, Revision B.3: Frisch, M. J.; Trucks, G. W.; Schlegel, H. B.; Gill, P. M. W.; Johnson, B. G.; Robb, M. A.; Cheeseman, J. R.; Keith, T.; Petersson, G. A.; Montgomery, J. A.; Raghavachari, K.; Al-Laham, M. A.; Zakrzewski, V. G.; Ortiz, J. V.; Foresman, J. B.; Peng, C. Y.; Ayala, P. Y.; Chen, W.; Wong, M. W.; Andres, J. L.; Replogle, E. S.; Gomperts, R.; Martin, R. L.; Fox, D. J.; Binkley, J. S.; Defrees, D. J.; Baker, J.; Stewart, J. P.; Head-Gordon, M.; Gonzalez, C.; Pople, J. A. Gaussian, Inc., Pittsburgh, PA, 1995.
(30) Andzelm, J.; Klobukowski, M.; Radzio-Andzelm, R. *J. Compt. Chem.* **1984**, *5*, 146.
(31) Maroulis, G.; Thakkar, A. J. *Mol. Phys.* **1991**, *73*, 1235.
(32) Hotop, H.; Lineberger, W. C. *J. Phys. Chem. Ref. Data* **1985**, *14*, 731.
(33) Moore, C. E. *U.S. Natl. Stand. Circ. 467* **1958**, *Vol. III*.
(34) Bowmaker, G. A.; Schwerdtfeger, P. *J. Mol. Struct. (THEOCHEM)* **1989**, *184*, 87.
(35) David, D.; Hrušák, J.; Shaik, S. *Chem. Phys. Lett.* **1995**, *233*, 249.
(36) Maslen, P. E.; Faeder, J.; Parson, R. *Chem. Phys. Lett.*, in press.
(37) Tripathi, G. N. R.; Schuler, R. H.; Fessenden, R. W. *Chem. Phys. Lett.* **1985**, *113*, 563.
(38) Chen, E. C.; Wentworth, W. E. *J. Phys. Chem.* **1985**, *89*, 4099 and references therein.
(39) Nadal, M. Ph.D. Thesis, University of Colorado, 1996.
(40) Sharp, S.; Gellene, G. I. Manuscript in preparation.
(41) Huber, K. P.; Herzberg, G. *Constants of Diatomic Molecules*, Van Nostrand Reinhold: New York, 1979.
(42) Teichteil, C.; Pelissier, M. *Chem. Phys.* **1994**, *180*, 1.
(43) Topol, L. E. *Inorg. Chem.* **1971**, *10*, 736.
(44) Sutherland, L. Private communication.
(45) Parrett, F. W.; Taylor, N. J. *J. Inorg. Nucl. Chem.* **1970**, *32*, 2458.
(46) Broekema, J.; Havinga, E. E.; Wiebenga, E. H. *Acta Crystallogr.* **1957**, *10*, 596.
(47) Stirling, A. *J. Chem. Phys.* **1996**, *104*, 1254.
(48) Nour, E. M.; Chen, L. H.; Laane, J. *J. Phys. Chem.* **1986**, *90*, 2841.
(49) Andrews, L.; Prochaska, E. S.; Loewenschuss, A. *Inorg. Chem.* **1980**, *19*, 463.